JOINT EUROPEAN TORUS

JET–P(91)29

M. Hugon, B. Ph van Milligen, P. Smeulders, L. Appel, D. Bartlett,
D. Boucher, A. Edwards, L. Eriksson, C. Gowers, T.C. Hender, G Huysmans,
J. Jacquinot, P. Kupschus, L. Porte, P.H. Rebut, D. Start, F. Tibone,
B.J.D. Tubbing, M. Watkins, W. Zwingmann and JET Team

Shear Reversal and MHD Activity during Pellet Enhanced Performance Plasmas in JET

Shear Reversal and MHD Activity during Pellet Enhanced Performance Plasmas in JET

M. Hugon, B. Ph van Milligen[1], P. Smeulders, L. Appel[2], D. Bartlett, D. Boucher, A. Edwards, L. Eriksson, C. Gowers, T.C. Hender[2], G Huysmans[1], J. Jacquinot, P. Kupschus, L. Porte[3], P.H. Rebut, D. Start, F. Tibone, B.J.D. Tubbing, M. Watkins, W. Zwingmann and JET Team*

JET-Joint Undertaking, Culham Science Centre, OX14 3DB, Abingdon, UK

[1]FOM Instituut voor Plasma Fysica "Rijnhuizen" PO Box 1207, 3430 BE Nieuwegein, The Netherlands
[2]UKAEA I Euratom Fusion Association Culham Laboratory, Abingdon, Oxfordshire OX14 3DB, UK
[3]University of Strathclyde, Glasgow Gl 1BA, UK
** See Appendix 1*

Preprint of Paper to be submitted for publication in
Nuclear Fusion

Shear reversal and MHD activity during Pellet Enhanced Performance plasmas in JET

M. Hugon, B.Ph. van Milligen[1], P. Smeulders, L. Appel[2], D. Bartlett, D. Boucher, A. Edwards, L. Eriksson, C. Gowers, T.C. Hender[2], G. Huysmans[1], J. Jacquinot, P. Kupschus, L. Porte[3], P.H. Rebut, D. Start, F. Tibone, B.J.D. Tubbing, M. Watkins, W. Zwingmann

JET Joint Undertaking
Abingdon, Oxfordshire OX14 3EA, United Kingdom

[1] FOM Instituut voor Plasma Fysica "Rijnhuizen"
PO Box 1207, 3430 BE Nieuwegein, The Netherlands

[2] UKAEA / Euratom Fusion Association
Culham Laboratory, Abingdon, Oxfordshire OX14 3DB, United Kingdom

[3] University of Strathclyde, Glasgow G1 1BA, United Kingdom

Abstract

Analysis of MHD activity in Pellet Enhanced Performance (PEP) pulses is used to determine the position of rational surfaces associated with the safety factor q. This gives evidence for negative shear in the central region of the plasma. The plasma equilibrium calculated from the measured q values yields a Shafranov shift in reasonable agreement with the experimental value of about 0.2 m. The corresponding current profile has two large off-axis maxima in agreement with the bootstrap current calculated from the electron temperature and density measurements. A transport simulation shows that the bootstrap current is driven by the steep density gradient, which results from improved confinement in the plasma core where the shear is negative. During the PEP phase (m,n) = (1,1) fast MHD events are correlated with collapses in the neutron rate. The dominant mode preceding these events usually is n = 3, whereas the mode following them is dominantly n = 2. Toroidal linear MHD stability calculations assuming a non-monotonic q-profile with an off-axis minimum decreasing from above to below 1 describe this sequence of modes (n = 3, 1, 2), but always give a larger

growth rate for the n = 1 mode than for the n = 2 mode. This large growth rate is due to the high central poloidal beta of 1.5 observed in the PEP pulses. Finally, a rotating (m,n) = (1,1) mode is observed as a hot spot with a ballooning character on the low field side. The hot spot has some of the properties of a 'hot' island consistent with the presence of a region of negative shear.

1. Introduction

A regime of enhanced performance in tokamaks can be accessed by deep pellet injection leading to strongly peaked density profiles in centrally heated plasmas, as first proposed in [1, 2, 3]. This regime has been achieved in JET by injection of deuterium pellets into L-mode limiter ICRF heated plasmas [4]: it is known as the pellet-enhanced performance (PEP) mode. Similar results, but with neutral beam heating, have been obtained in DIII [5], JT60 [6] and JFT 2-M [7].

Compared to similar non-PEP pulses the PEP mode is characterized by a substantial increase of the neutron rate (by about 5 times), a very strong peaking of the electron density n_e and kinetic pressure near the plasma centre and a relatively small increase of the global energy confinement time τ_E (by about 20%). The PEP mode is a transient phenomenon, lasting typically 1 to 2 s. It is terminated by a rapid loss of central pressure, often associated with MHD phenomena. It has been suggested [4] that the abrupt termination of the PEP mode could be associated with the presence of a potentially unstable non-monotonic profile of the safety factor q. The negative shear region in the plasma core is thought to be created by a substantial bootstrap current. The central electron and ion thermal conductivities derived from the experimental data are reduced by a factor 2 - 3 with respect to the usual anomalous values [8]. This reduction of transport parameters could be due to the existence of negative shear in the plasma centre [9].

More recently, in JET the PEP mode has been combined with an H-mode [10, 11]. These shots have produced large values of thermonuclear neutron rate of approximately 10^{16} s^{-1} and fusion product $n_D(0)T_i(0)\tau_E \approx 7 \cdot 10^{20}$ m^{-3} keV s in plasmas having nearly the same electron and ion temperatures ($T_e \approx T_i \approx 10$ keV). The projected deuterium-tritium fusion rate in JET is much larger in the PEP mode than in non-enhanced plasmas. In next-step devices, the transient PEP-H mode could be used to ignite the plasma.

It is therefore of great interest to have a better understanding of the MHD behaviour, plasma equilibrium and transport to improve the performance during the PEP phase. This

paper reports on the analysis of MHD activity measured by several diagnostics at a high sampling rate in the recent PEP-H mode plasmas. Section 2 gives a brief description of the diagnostics and of the data analysis methods involved. Section 3 discusses the experimental results and their theoretical interpretation and conclusions are given in Section 4. A typical PEP-H mode pulse is described in Section 3.1 and the MHD behaviour during the PEP phase is discussed in Section 3.2. The position of rational q-surfaces obtained from MHD mode analysis provides experimental evidence for negative shear in the plasma core and this is presented in Section 3.3. A PEP plasma is simulated using a predictive time dependent 1-D transport code in Section 3.4. The MHD modes observed during the PEP phase are compared with the predictions of two toroidal linear MHD codes in Section 3.5. In Section 3.6 the topology of a rotating (m,n) = (1,1) mode is analyzed in detail in the region of negative shear.

2. Diagnostics and data analysis

2.1 Diagnostics

The study of MHD activity in JET involves many diagnostics which are located at different poloidal and toroidal positions. The JET vacuum vessel consists of 8 octants, numbered from 1 to 8 in the counterclockwise direction as seen from the top. The following diagnostics have been used in these studies:

• Magnetic diagnostic: the poloidal field is measured by a poloidal set of 18 pick-up coils in octant 4 and a toroidal set of 8 such coils located on the outboard side above the midplane inside the vacuum vessel. Each coil has a frequency cutoff at 10 kHz with a slope of 6 dB per octave. In addition, a hardware combination of pick-up coils at different toroidal locations allows measurement of the toroidal mode number n of rotating magnetic modes up to n = 4.

• Polychromator: a 12-channel grating polychromator measures the electron temperature locally from the 2^{nd} harmonic extraordinary mode electron cyclotron emission (ECE) on a horizontal chord in the midplane in octant 7 [12]. The spatial resolution is approximately 0.06 m radially and 0.15 m in the transverse direction.

• Radiometer: the electron temperature is also measured by a 44-channel microwave heterodyne radiometer from the 1^{st} harmonic ordinary mode ECE on a horizontal chord in the midplane in octant 7 [13]. This emission may suffer from cutoff at the plasma frequency in high density pulses. Its spatial resolution is approximately 0.02 m radially and 0.15 m in the transverse direction.

• Soft X-rays: the soft X-ray diagnostic is equipped with a 38-channel vertical camera and a 62-channel horizontal camera in octant 2 and 16 toroidal diodes (4 of each in octants 1, 3, 5 and 6 at various elevations above the midplane) [14]. The transverse resolution is 0.07 m in the midplane for the vertical cameras.

• LIDAR: the LIDAR time-of-flight Thomson scattering diagnostic measures the electron density and temperature profiles every 1.2 s along a horizontal chord in the mid-plane of octant 5 [15].

2.2 *Data analysis and correlation between diagnostics*

It is difficult to determine the poloidal mode number m from the poloidal set of pick-up coils, because the signals are affected by the D-shape of the vacuum vessel, the shape of the plasma for double null discharges and the plasma position. In addition, the pick-up coils measure the combined effects of all modes present in the plasma with a weight which depends on their relative amplitude, radial position and mode number. In the PEP pulses, most of the MHD activity takes place in the central region of the plasma, making the mode number analysis for these central modes very difficult.

The soft X-ray diagnostic provides a powerful tool for local mode number determination. From the toroidal cameras in combination with a selection of horizontal channels it it possible to determine the toroidal mode numbers up to n = 4. Analysis of the horizontal and vertical camera raw data can yield mode numbers up to m = 4. In addition, a static 2-dimensional tomographic reconstruction technique can distinguish between poloidal mode numbers m = 0, 1 and 2 [16]. If m = 0 (m = 1) can be excluded, m = 4 (m = 3) can be assumed taking into account the symmetries appearing in both cameras and also the properties of the q-profile. A single-camera (vertical or horizontal) rotational tomographic reconstruction technique is also available, which can handle mode numbers up to m = 4 [17].

In correlating the data measured by the various diagnostics, care has been taken to take proper account of their relative timing and position. In the present study the direction of the toroidal magnetic field is counterclockwise and the plasma current is in the clockwise direction as seen from the top of the vacuum vessel, which determines the helicity of the magnetic field. Knowledge of the direction of rotation, frequency and mode numbers of an observed mode is essential for the correlation. For diagnostics located in the midplane it is only necessary to know the toroidal mode number, assuming that the plasma rotation is purely toroidal.

3. Results and discussion

3.1 A typical PEP-H mode pulse

The PEP-H mode pulses investigated here are obtained by injecting one or several pellets into double null plasmas during the current rise before the q-profile has fully evolved. Fig. 1 shows the time variation of signals characterizing a typical PEP-H mode plasma (Pulse No.23107). The toroidal magnetic field is 2.9 T. The plasma current reaches a constant value of 3.6 MA at 6.0 s. The X-points are formed at 4.0 s, marked by an increase in the D_α signal. Deuterium pellets are injected at 4.75 s (2.7 mm) and at 5.0 s (4.0 mm), causing a decrease in electron temperature T_e and a sharp increase in the central density $n_e(0)$ and the D_α signal. The 4mm pellet causes a strong peaking of the density profile indicating the beginning of the PEP mode as can be seen in Fig.1c. Subsequently the electron density decreases gradually. At 5.5 s, the ICRF heating is ramped up to 9 MW. In this particular pulse NBI heating is not applied. During the PEP-L phase, the electron and ion temperatures and the neutron rate increase sharply from the moment ICRF heating is applied. At 5.9 s there is an L to H transition, indicated by a slight decrease in the D_α signal. During the PEP-H phase the neutron rate reaches a peak value of $6 \cdot 10^{15}$ s^{-1}. At 6.35 s a central n = 1 MHD event terminates both the PEP phase and the H-mode and the plasma energy content W_{DIA} decreases sharply. It should be noted that in many pulses the PEP phase terminates before the end of the H-mode. The PEP phase always takes place well before the onset of the ordinary sawtooth activity (about 8 s in these shots). The H to L transition can be seen from an increase in the D_α signal and a drop in $\langle n_e \rangle$. The PEP phase can be diagnosed by the evolution of the soft X-ray centroid radius, R_{SXR}, which is closely related to the magnetic axis radius, R_{mag}. R_{SXR} is the position of the maximum of the soft X-ray emission profile in the midplane as determined by means of the static tomography technique. R_{SXR} is observed to move strongly outward after starting the ICRF heating due to the build-up of central pressure caused by the central temperature increase at high density. At 6.35 s, a sudden inward movement is observed corresponding to the termination of the PEP phase.

3.2 MHD behaviour during the PEP phase

During the PEP phase, collapses in the neutron rate occur that are often correlated with fast MHD events. From the soft X-ray measurements most of these events are found to have (m,n) = (1,1) mode numbers. The n = 1 mode number is confirmed by the magnetic pick-up coils. From the soft X-ray and the magnetic diagnostics it is found that rotating modes

preceding the (1,1) event by several tens of ms generally have an n = 3 mode number. In some cases, their poloidal mode number is determined to be m = 4 from soft X-ray emission analysis. Often a fast-growing rotating n = 2 mode starts already in the precursor phase of the fast event with a frequency twice that of the n = 1 mode, indicating that the n = 2 mode arises as a non-linear consequence of the n = 1 mode [18]. After the fast event, generally the n = 1 mode amplitude decreases strongly and a dominant n = 2 mode is observed with a weak n = 3 mode. Fig. 2 shows a typical example of this behaviour observed in Pulse No.23100. Impurity radiation at the plasma edge is enhanced by the crash. The resulting impurity influx may lead to a long-term dilution of deuterium in the plasma core and a decrease of the neutron rate. Note that the central ion (from charge exchange measurements) and electron temperatures remain approximately constant during these crashes, indicating that the D-D cross section is not affected.

3.3 Determination of the q-profile

Fig. 3 shows the behaviour of the electron temperature T_e at various positions in the plasma as seen by the polychromator (Pulse No. 23100). As discussed in the previous section, the fast event at 6.542 s is an n = 1 mode, which is preceded by a dominant n = 3 mode and followed by dominant n = 2 modes. The (1,1) fast MHD event does not affect the central electron temperature. Note the non-sinusoidal character of the oscillations after this event and the slight phase shift between the channels at R = 3.56 and R = 3.64 m, suggesting that distinct but coupled modes (on different rational surfaces) may be involved. There is an error of about 0.1 m in the absolute value of the major radii corresponding to the polychromator channel positions. This is due to the uncertainty in calculating the total magnetic field for these plasmas with a large bootstrap current and a total current which has not reached a steady state (see below). The n = 2 modes last about 200 ms until a fast MHD event terminates the PEP phase. The electron temperature oscillations are in phase with the poloidal field oscillations for the n = 3 and n = 2 modes as expected for rotating magnetic islands.

Fast soft X-ray data (sampling at 200 kHz) allow determination of the mode numbers of the oscillations after the n = 1 event. The soft X-ray centroid radius, R_{SXR} = 3.30 m, indicates a large Shafranov shift. Detailed analysis reveals a (3,2) mode of small amplitude at r = 0.14 m and a (2,2) mode of large amplitude at r = 0.25 m. The effective relative amplitudes of the oscillations are plotted as a function of minor radius in Fig. 4. Taking into account the variation in the measured Shafranov shift, the rational surfaces are believed to be at R = 3.15 and 3.42 m for the (3,2) mode and R = 3.02 and 3.52 m for the (2,2) mode. This

shows that the shear is negative in the central region of the plasma. The error in the allocation of the maximum amplitude of a mode is typically the spacing between two diodes, which is of the order of 0.05 m. The radial displacement of the (2,2) and (3,2) modes has a maximum of about 0.05 m and extends over around 0.15 m of the plasma.

The positions of the rational surfaces deduced from the soft X-ray measurements after the n = 1 event are used as additional constraints on the plasma equilibrium calculated by the IDENTD code [19]. The equilibrium identification is done by minimizing a cost function that evaluates the deviation between simulated and observed measurements with the constraint of the Grad-Shafranov equation. IDENTD accommodates measurements of 14 flux loops and 18 pick-up coils at the vacuum vessel, the plasma current, the diamagnetic signal, the total pressure and safety factor at discrete points. The magnetic flux at the position of the flux loops is used directly as a boundary condition for the Grad-Shafranov equation and the total plasma current I_p is equal to the surface integral of the current density. All other quantities are fitted via minimization of the cost function. The total pressure is approximated by $p = \alpha p_e$ with the constant factor α of the order of 2 and p_e is the electron pressure from LIDAR (see Fig. 5d). The electron temperature T_e is approximately equal to the ion temperature T_i as shown in Fig. 1. The remaining uncertainty on the pressure is taken into account by choosing a low weight in the cost function.

The calculated q-profile is shown in Fig.5a. The discrepancy between the q-profile and the positions of the rational surfaces deduced from the observed mode activity on the high field side is partly due to a convergence problem of the algorithm when an attempt is made to enforce better agreement with the measurements. In addition, the flux surfaces are assumed to be concentric ellipses (i.e. in-out symmetric) in the soft X-ray reconstruction used to determine the island positions, whereas the q-profile is asymmetric because of the large Shafranov shift. The soft X-ray centroid radius is R_{SXR} = 3.30 m and the position of the maximum in the electron pressure is at R = 3.28 m (see Fig. 5d), both comparing fairly well with the magnetic axis radius calculated by IDENTD (R_{mag} = 3.21 m).

The current density j obtained from IDENTD computations is shown in Fig.5b. Note that the central current density is too low by about 20% from the value of q(0) shown in Fig.5a: this is due to a numerical problem of the equilibrium code, when computing strongly hollow j-profiles. The innermost 'twin peaks' of the j-profile are correlated with the steep density gradients in the central region (see Fig.5c). Fig. 5b also shows the bootstrap current contribution to the total current as computed from the LIDAR data [20]. The radial position and

amplitude of the calculated bootstrap current matches the deviation of the reconstructed current profile from a roughly parabolic profile having the same central current density.

3.4 Transport simulation of the PEP mode

The evolution of temperature, current and density profiles of Pulse No. 23100 has been simulated using a predictive time dependent 1-D transport code [21] based on the critical temperature gradient model of plasma transport [9]. The simulations provide insight into the formation of the region of negative shear and into the consequences for transport within this region.

The computation starts just before the injection of the first pellet at 4.75s. A large region (about 40% of the minor radius) with slightly negative shear is created after the injection of the second and last pellet at 5s by a combination of three factors: (i) the broad current and q-profiles in the early phase; (ii) the transient inversion of the temperature profile and consequently of the current profile by the pellet injection; (iii) a small bootstrap current driven mainly by the density gradient. The region of negative shear is maintained during the 1 second of ohmic heating and weak ICRF heating (about 1.5MW). After the onset of additional power (10MW ICRH and 2.5MW NBI), the bootstrap current increases strongly producing a more hollow q-profile. Fig.6a compares the simulated q-profile at 6.6s with that obtained from IDENTD computations: there is a reasonable agreement, bearing in mind that the transport code is 1-D, with nested circular flux surfaces that take little account of elongation or shifts in the magnetic axis, which are considered elsewhere [22].

The calculated temperature and density profiles are in good agreement with the LIDAR profiles at 6.6s (see Fig.6b) and time variations of the central electron temperature (Fig.6d) and neutron yield (Fig.6e) are also well reproduced. In line with the critical electron temperature gradient model, it is necessary to reduce ion heat conduction and particle transport to neoclassical levels within the region of reversed shear. It is also necessary to reduce the electron transport to about 0.5 to 1 times ion neoclassical values, that is, comparable to electron neoclassical levels, is poloidal variations in the electric potential are important [23]. The reduced transport inside the region of negative shear is shown in Fig. 6c by the lower thermal conductivities. Outside this region experimental data are well represented by the anomalous transport of the critical electron temperature gradient model. The conclusions of this simulation are similar to those obtained previously for other pulses with a predictive 1-1/2-D equilibrium-transport code [22].

3.5 Mode stability computation

To see how the n = 3,1,2 sequence of modes observed in Pulse No.23100 compares with theory, a series of toroidal MHD calculations have been performed. For these calculations the resistive linear MHD code FAR [24] is used. The equilibria are specified by defining the plasma boundary shape and the pressure and q profiles. The plasma boundary shape, determined from external magnetic measurements, has an elongation of 1.67 and a triangularity of 0.27. The pressure profile is obtained from the LIDAR data and its magnitude is adjusted to match the measured diamagnetic pressure to take into account the ion contribution. The average β_p is 0.29 during the n = 3 activity and is 0.38 during the n = 1 and 2 activity. The q-profile is constrained to match the experimental total plasma current, which essentially determines the edge q. The central q is fixed at 1.6 and a sequence of q-profiles is considered ranging from slightly to strongly non-monotonic, with a minimum q_{min} at r/a = 0.3, as shown in the inset in Fig. 7. This series of q-profiles is consistent with the experimental data discussed in Section 3.3: the soft X-ray analysis indicates that the q-profile is inverted with q = 3/2 and q = 1 rational surfaces at r = 0.14 m and 0.25 m respectively after the fast (m,n) = (1,1) MHD event; in addition, the off-axis minimum of q is well above 1 just after pellet injection and decreases slowly towards a value below 1 as shown by the change from (m,n) = (4,3) to (2,2) activity. The results of the computation of the n = 1,2,3 growth rates (normalized to the poloidal Alfvén time $\tau_A \approx 0.2$ μs) are plotted in Fig. 7 versus q_{min}. These calculations are resistive with a magnetic Reynolds number (as defined in [24]) of $s = 10^6$. The n = 1 and 2 modes are ideally unstable kinks as is the n = 3 mode for $q_{min} \lesssim 1.15$. It can be seen from Fig.7 that as q_{min} decreases the instabilities appear in the correct experimental sequence n = 3,1,2. A difficulty is that the n = 2 mode always grows more slowly than the n = 1 mode contrary to the experimental observation. It may be that a nonlinear simulation or the addition of terms not included in the MHD model could make the n = 2 mode dominant for $q_{min} \lesssim 1$. The very large growth rate of the n = 1 mode for $q_{min} \lesssim 1.1$ arises because the central poloidal beta [25] calculated from the LIDAR pressure profile is about 1.5, well above the critical value of around 0.3 when $q_{min} \approx 1$.

As the q-profile is not directly determined during the n = 3 activity, the sensitivity of the n = 3 growth rate to variations of q has been examined. For example, when raising the central q to 2, the dependence of the n = 3 growth rate on q_{min} is very similar to that shown in Fig. 7, though its maximum is 25% larger. It can thus be concluded that the n = 3 results are not very sensitive to details of the q-profile within the likely experimental range.

The growth rates of the n = 1, 2 and 3 modes have also been computed with the toroidal linear resistive MHD code CASTOR [26]. The results of the calculation confirm those obtained with the FAR code.

The question arises what is the effect of fast ions produced by ICRF heating on the stability of the m = 1 kink during the PEP mode. For Pulse No. 23100, the ICRF heating power is of the order of 10 MW and creates a significant fraction of fast ions; their total energy, calculated using a Fokker-Planck code, is of the order of 0.5 - 1.0 MJ, compared to about 6 MJ for the total plasma energy. The computed kinetic energy of the fast ions is in the range 100 - 200 keV, when the q = 1 surface appears in the plasma. The radial profile of their energy density is found to have its maximum within 0.03 m of the magnetic axis and to be almost zero at 0.3 m from the magnetic axis. Thus, most of the fast ions are located within the q = 1 surface measured at 0.25 m (see Section 3.3). Under these conditions, for the non-monotonic q-profile observed during the PEP mode, the fast ions should be destabilizing for the m = 1 kink, when q_{min} is just above 1 [27].

3.6 Topology of a rotating (m,n) = (1,1) mode

Fig. 8 shows the temporal behaviour of the electron temperature from the ECE radiometer (Pulse No. 23103). The oscillations at R = 3.61 m are of large amplitude and appear in a few channels only, indicating that they are localized radially, and show non-sinusoidal behaviour. They are located in a region where the electron temperature gradient is very steep. The toroidal mode number measured by the magnetic pick-up coils is n = 1 and the poloidal mode number is m ≈ 5 due to mode coupling. We have performed a correlation analysis between the temperature (from the ECE radiometer) and poloidal magnetic field oscillations, taking into account the toroidal separation of these diagnostics and the n = 1 symmetry of the mode: the maximum in electron temperature corresponds to a maximum in poloidal field. From SXR fast data (200 kHz sampling) we find that the central dominant mode is (m,n) = (1,1). The temperature maximum corresponds to a maximum in soft X-ray emission. The mode rotates counter-clockwise toroidally, i.e. in the direction of the electron diamagnetic drift and opposite to the neutral beams. In addition, the measurements from the vertical camera displayed in Fig. 9 indicate that the mode has a ballooning character: it is stronger on the low field side (channel 27) than on the high field side (intermediate between channels 18 and 19). The soft X-ray centroid has a radius $R_{SXR} \approx 3.30$ m.

The soft X-ray rotational tomographic reconstruction (Fig. 10) displays the (1,1) mode at r ≈ 0.22 m. The rotating structure has a small poloidal extent and does not affect the core of

the plasma. It corresponds to a radial displacement, which has a maximum of around 0.05 m and extends over about 0.1 m of the plasma. It could be interpreted as the O-point of a (1,1) island.

The soft X-ray measurements suggest the existence of another mode near the plasma centre ($r \approx 0.1$ m), which has tentatively been identified as (m,n) = (2,1). A plasma equilibrium with a central value of q around 2 can indeed be obtained with the IDENTD code; so a (2,1) island cannot be excluded close to the magnetic axis.

Magnetic islands can be sustained by a current perturbation δj flowing inside. In this case, the core of the island with nested surfaces is expected to have a smaller poloidal extension than the region surrounding the X-points of the separatrix, which is easily destroyed by chaos, since filaments carrying parallel current attract each other. From Ampère's law, it follows that the current perturbation δj inside the island is opposite to the main plasma current j when the shear q' is positive and in the same direction as j when q' is negative. If the current perturbation δj is due to a thermal instability inside the island, it depends on the electron temperature through the resistivity and Ohm's law. The resulting island is then colder than the surrounding plasma when q' is positive and warmer when q' is negative [28]. It follows that the electron temperature oscillations associated with a rotating thermal island measured at a fixed location in the plasma are expected to be non-sinusoidal: for a 'hot' island, the maximum is of shorter duration than the minimum.

The non-sinusoidal behaviour of the oscillations observed by the ECE and soft X-ray diagnostics seems to suggest at first the (1,1) mode structure is a 'hot' island. This agrees with the existence of negative shear in the central region of the plasma as inferred above. However, the ballooning character of the (1,1) mode observed experimentally is not explained by the thermal island model [28]. In addition, from the shear computed by IDENTD of $q' \approx -5$ m^{-1} and the relative temperature oscillation amplitude $\delta T_e/T_e \approx 0.5$ at the island position, the width calculated for a thermal island is about 0.5 m, much larger than that observed. Although there is a large uncertainty in the shear determination, this calculation suggests that the island could be strongly stabilized by some mechanism reducing its width such as bootstrap current in the region of negative shear.

There remains the difficulty that the ideal MHD internal kink should be violently unstable when the off-axis minimum of q is less that unity (see Fig. 7). Thus, if the (1,1) mode is a true island, the internal kink must be stabilized by some unidentified mechanism or by a nonlinear process taking into account the change in topology due to the presence of the island. Alternatively, the (1,1) mode might be a local distortion of the flux surfaces with the

minimum in q just below the marginal value for the n = 1 mode destabilization (≈ 1.1 for the case shown in Fig. 7). However, the topology of the nonlinearly saturated state computed in [29] does not evidently explain the observation of a localized hot spot on the low field side.

4 Conclusions

MHD modes occurring during the Pellet Enhanced Performance (PEP) mode have been studied in this paper. Analysis of soft X-ray data has led to the determination of the position of rational q-surfaces, showing that the shear is negative in the central region of the plasma. In a particular pulse, (m,n) = (3,2) and (2,2) modes are found at radii r = 0.14 and 0.25 m respectively. The measured positions of the q = 1 and q = 1.5 surfaces are used as additional constraints to the plasma equilibrium which shows a Shafranov shift in reasonable agreement with that obtained from the soft X-ray measurements (about 0.2 m). The calculated current profile displays large off-axis peaks consistent with the bootstrap current computed from the measured electron density and temperature profiles. A predictive time dependent 1-D transport code shows that the bootstrap current is maintained by the improved confinement in the central region of the plasma where the shear is negative: the ion transport coefficients are reduced to their neoclassical values in line with the critical electron temperature gradient model; electron transport coefficients also have to be reduced within this region and in this case are set to about 0.5 to 1 times ion neoclassical levels.

During the PEP phase fast (m,n) = (1,1) MHD events often occur close to the maximum in the neutron rate. These events are usually preceded by n = 3 modes and followed by dominant n = 2 modes. This sequence of modes (n = 3, 1, 2) appears in calculations obtained with two different toroidal linear MHD codes assuming a non-monotonic q-profile with an off-axis minimum q_{min} which is decreasing from above to below 1. However, the n = 2 mode is always less unstable than the n = 1 mode, contrary to the experiment. The large growth rate calculated for the n = 1 mode for $q_{min} \lesssim 1.1$ is due to the high value of the central poloidal beta of 1.5 characteristic of the PEP mode. A rotating (m,n) = (1,1) mode has been studied in detail: it has the appearance of a localized hot spot ballooning at the low field side of the plasma. This hot spot has some characteristics of a 'hot' island consistent with the presence of negative shear in the plasma core. Both experimental observations (n = 2 mode after the (1,1) MHD event and hot spot) suggest that the internal kink is strongly stabilized by some mechanism or by a nonlinear process taking into account the change in topology due to the presence of islands.

Acknowledgements

The authors are very grateful to B. Balet, H. de Blank, C.D. Challis, S. Corti, A.E. Costley, J. Ellis, J. Fessey, G. Fishpool, R. Gill, N. Gottardi, M. von Hellermann, B. Keegan, E. Lazzaro, P. Morgan, C. Nardone, G. Neill, H. Oosterbeek, J. O'Rourke, D. Pasini, F. Porcelli, C. Sack, G. Sadler, C.S. Schüller, G. Sips, A. Taroni, J. Wesson and S. Wolfe for providing experimental data, helping with data analysis or for fruitful discussions. The authors acknowledge the support of the entire JET Team. Part of this work was performed under the Euratom-FOM Association agreement, with financial support from NWO and Euratom.

References

[1] H.P. FURTH, Plasma Physics and Controlled Fusion, **28** (1986) 1305.

[2] P.H. REBUT AND JET TEAM, in Plasma Physics and Controlled Nuclear Fusion Research 1986 (Proc. 11th Int. Conf. Kyoto, 1986), Vol. 1, IAEA, Vienna (1987) 31.

[3] G.L. SCHMIDT, S.L. MILORA, V. ARUNASALAM, *et al.*, in Plasma Physics and Controlled Nuclear Fusion Research 1986 (Proc. 11th Int. Conf. Kyoto, 1986), Vol. 1, IAEA, Vienna (1987) 171.

[4] G.L. SCHMIDT AND JET TEAM, in Plasma Physics and Controlled Nuclear Fusion Research 1988 (Proc. 12th Int. Conf. Nice, 1988), Vol. 1, IAEA, Vienna (1989) 215.

[5] S. SENGOKU, M. NAGAMI, M. ABE, *et al.*, Nucl. Fusion, **25** (1985) 1475.

[6] M. NAGAMI AND JT-60 TEAM, Plasma Physics and Controlled Fusion, **31** (1989) 1597.

[7] K. ODAJIMA, A. FUNAHASHI, K. HOSHINO, *et al.*, in Plasma Physics and Controlled Nuclear Fusion Research 1986 (Proc. 11th Int. Conf. Kyoto, 1986), Vol. 1, IAEA, Vienna (1987) 151.

[8] A. TARONI, B. BALET, *et al.*, in Plasma Physics and Controlled Nuclear Fusion Research 1988 (Proc. 12th Int. Conf. Nice, 1988), Vol. 1, IAEA, Vienna (1989) 367.

[9] P.H. REBUT, P. LALLIA, M.L. WATKINS, in Plasma Physics and Controlled Nuclear Fusion Research 1988 (Proc. 12th Int. Conf. Nice, 1988), Vol. 2, IAEA, Vienna (1989) 191.

[10] B.J.D. TUBBING, *et al.*, Nucl. Fusion **31** (1991) 839.

[11] P. KUPSCHUS, *et al.*, in Contr. Fus. and Plasma Phys. (Proc. 18th Eur. Conf. Berlin, 1991), Vol. 15C, European Physical Society (1991) I-1.

[12] B.J.D. TUBBING, E. BARBIAN, D.J. CAMPBELL, C.A.J. HUGENHOLTZ, R.M. NIESTADT, Th. OYEVAAR, H.W. PIEKAAR, in Contr. Fus. and Plasma Phys. (Proc. 12th Eur. Conf. Budapest, 1985), Vol. 9F, Part I, European Physical Society (1985) 215.

[13] L. PORTE, D.V. BARTLETT, D.J. CAMPBELL, A.E. COSTLEY,in Contr. Fus. and Plasma Phys. (Proc. 18th Eur. Conf. Berlin, 1991), Vol. 15C, European Physical Society (1991) IV-357.

[14] A.W. EDWARDS, H.-U. FAHRBACH, R.D. GILL, R. GRANETZ, E. OORD, G. SCHRAMM, S. TSUJI, A. WELLER, D. ZASCHE, Rev. Sci. Instrum. **57** (1986) 2142.

[15] H. SALZMANN, J. BUNDGAARD, A. GADD, *et al.*, Rev. Sci. Instrum. **59** (1988) 1451.

[16] R.S. GRANETZ, P. SMEULDERS, Nucl. Fusion **28** (1988) 457.

[17] P. SMEULDERS, Rep. IPP-2/252, Max Planck Institut für Plasmaphysik Garching (1983).

[18] P. SMEULDERS, D. BARTLETT, A. EDWARDS, G. FISHPOOL, T.C. HENDER, M. HUGON, B.Ph. van MILLIGEN, C. NARDONE, G. NEILL, L. PORTE, S. WOLFE, W. ZWINGMANN, in Contr. Fus. and Plasma Phys. (Proc. 18th Eur. Conf. Berlin, 1991), Vol. 15C, European Physical Society (1991) II-53.

[19] J. BLUM, E. LAZZARO, J. O'ROURKE, B. KEEGAN, Y. STEPHAN, Nucl. Fusion **30** (1990) 1475.

[20] S.P. HIRSHMAN, Phys. Fluids **31** (1988) 3150.

[21] D. BOUCHER, P.H. REBUT, M.L. WATKINS, in Contr. Fus. and Plasma Phys. (Proc. 18th Eur. Conf. Berlin, 1991), Vol. 15C, European Physical Society (1991) I-177.

[22] A. TARONI, Ch. SACK, E. SPRINGMANN, F. TIBONE, in Contr. Fus. and Plasma Phys. (Proc. 18th Eur. Conf. Berlin, 1991), Vol.15C, European Physical Society (1991) I-181.

[23] T. E. STRINGER, Phys. Fluids B3 (1991) 981.

[24] L.A. CHARLTON, J.A. HOLMES, V.E. LYNCH, B.A. CARRERAS, T.C. HENDER, Journal of Comp. Phys. **86** (1990) 270.

[25] M.N. BUSSAC, R. PELLAT, D. EDERY, J.L. SOULE, Phys. Rev. Lett. **35** (1975) 1638.

[26] W. KERNER, S. POEDTS, J.P. GOEDBLOED, G.T.A. HUYSMANS, B. KEEGAN, E. SCHWARZ, in Contr. Fus. and Plasma Phys. (Proc. 18th Eur. Conf. Berlin, 1991), Vol. 15C, European Physical Society (1991) IV-89.

[27] F. PORCELLI, *private communication* .

[28] P.H. REBUT, M. HUGON, in Plasma Physics and Controlled Nuclear Fusion Research 1984 (Proc. 10th Int. Conf. London, 1984), Vol. 2, IAEA, Vienna (1985) 197.

[29] J.A. HOLMES, B.A. CARRERAS, L.A. CHARLTON, V.E. LYNCH, R.J. HASTIE, T.C. HENDER, Phys. Fluids **31** (1988) 1202.

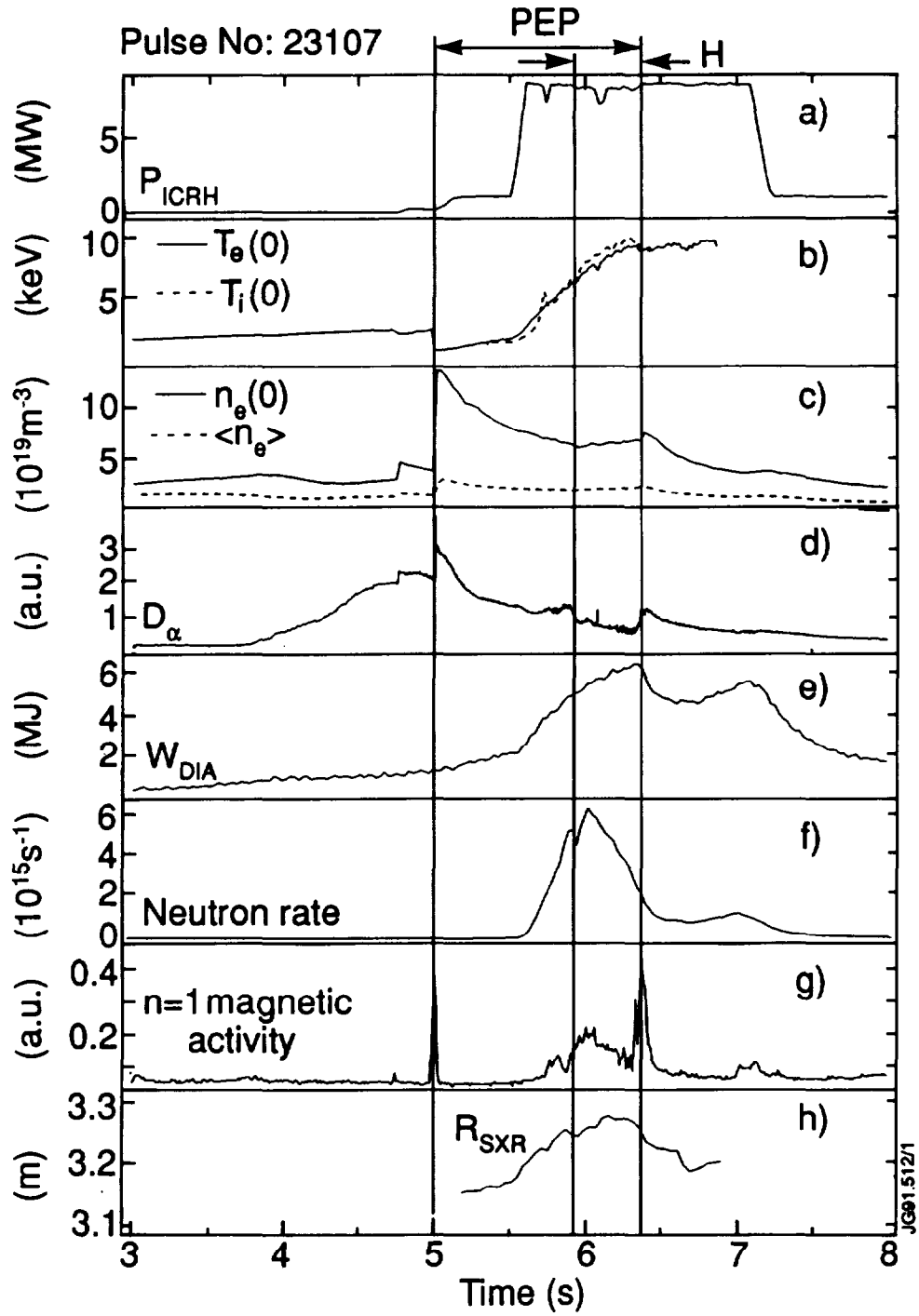

Fig.1 Time traces of some indicative quantities of a typical PEP plasma. Shown are: (a) the ICRH input power (there is no NBI in this pulse); (b) the central electron temperature from the ECE Michelson interferometer and the central ion temperature from He-like nickel radiation line-broadening; (c) the central and volume-average electron density from the far-infrared interferometer; (d) the D_α emission measured along a vertical chord viewing near the X-point region; (e) the total kinetic plasma energy derived from the diamagnetic loop measurements; (f) the total neutron rate; (g) the n = 1 magnetic activity; and (h) the soft X-ray centroid radius closely related to the magnetic axis radius.

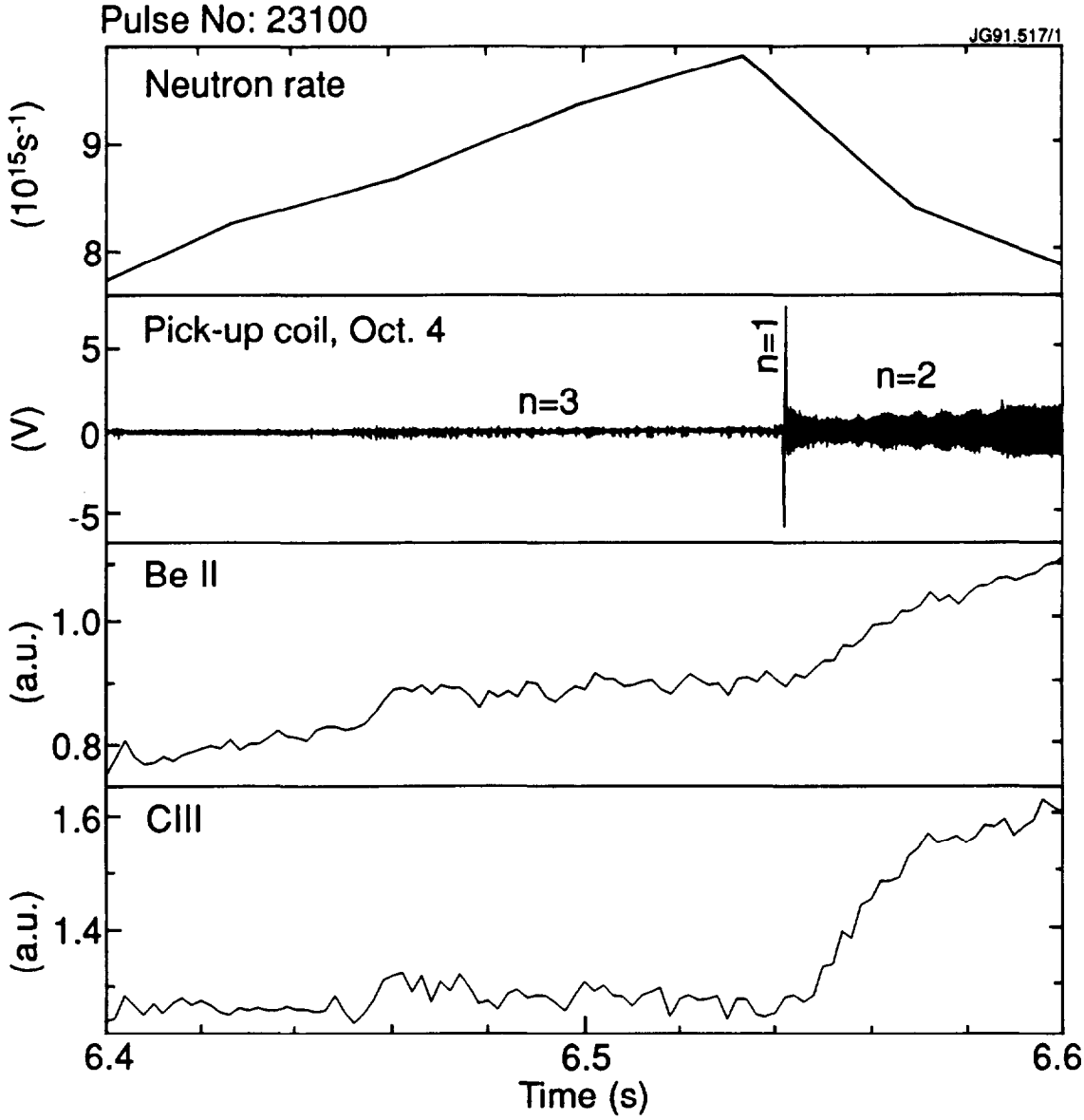

Fig.2 Time traces showing the neutron rate, the signal from a magnetic pick-up coil and the Be II and C III emissions measured on vertical chords through the plasma. Note that the decay in neutron rate coincides with the fast n = 1 MHD event. This event triggers impurity influx.

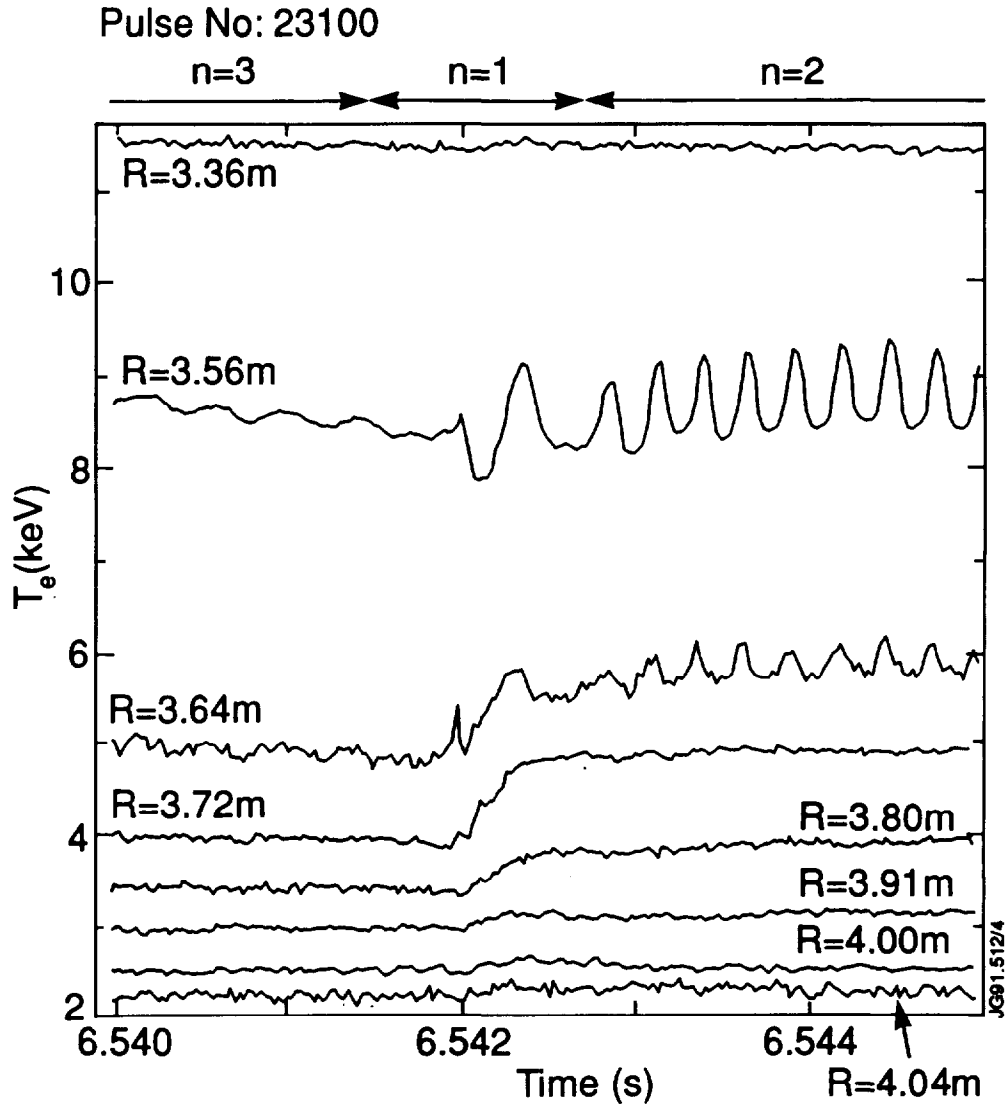

Fig.3 Time traces of the electron temperature from the ECE polychromator at various radii inside the plasma. The n = 1 event at 6.542 s is the same as the one shown in Fig. 2.

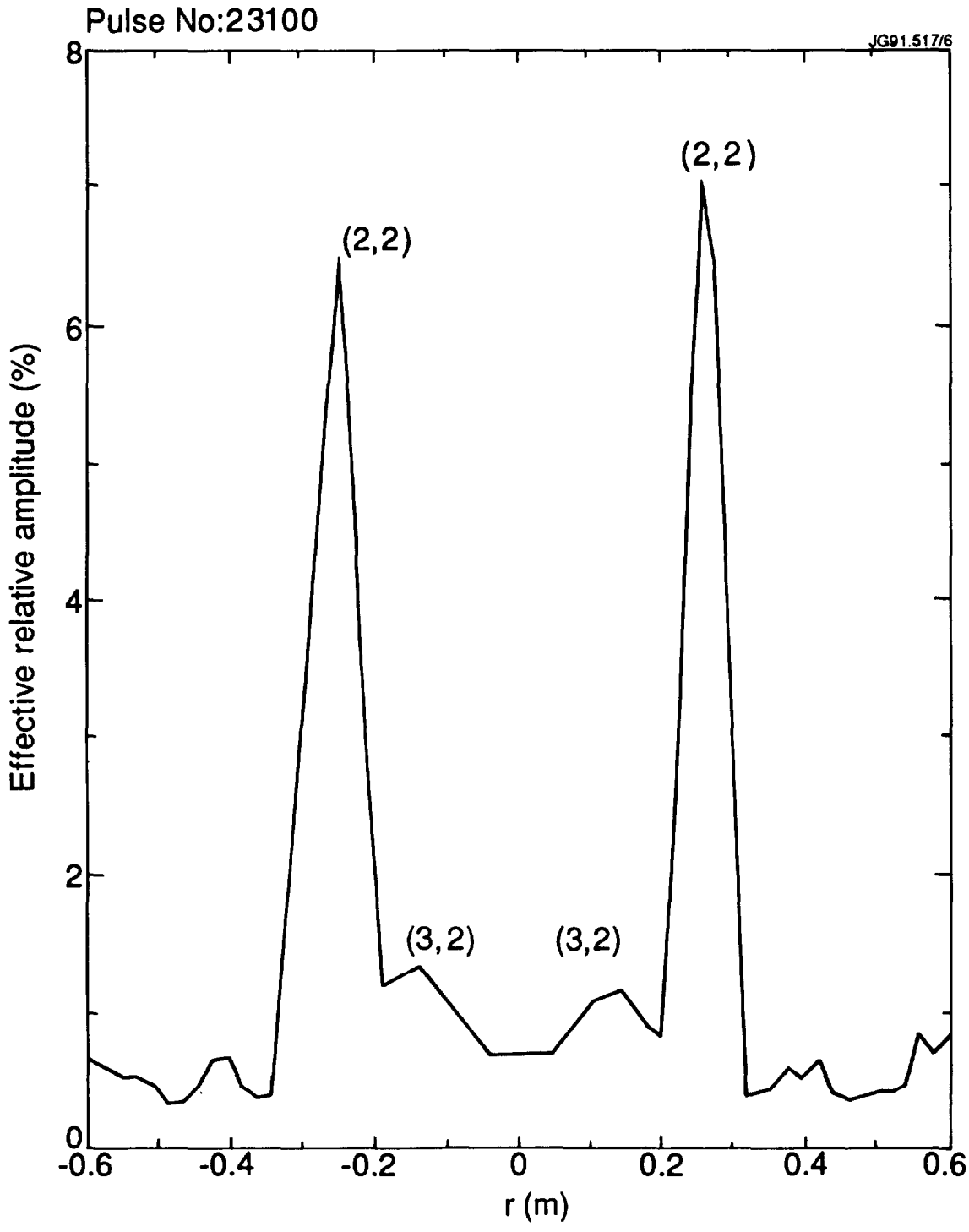

Fig.4 The effective relative amplitude of soft X-ray oscillations associated with rotating MHD modes versus horizontal minor radius as determined from rotational tomography. The corresponding mode numbers are indicated in the figure.

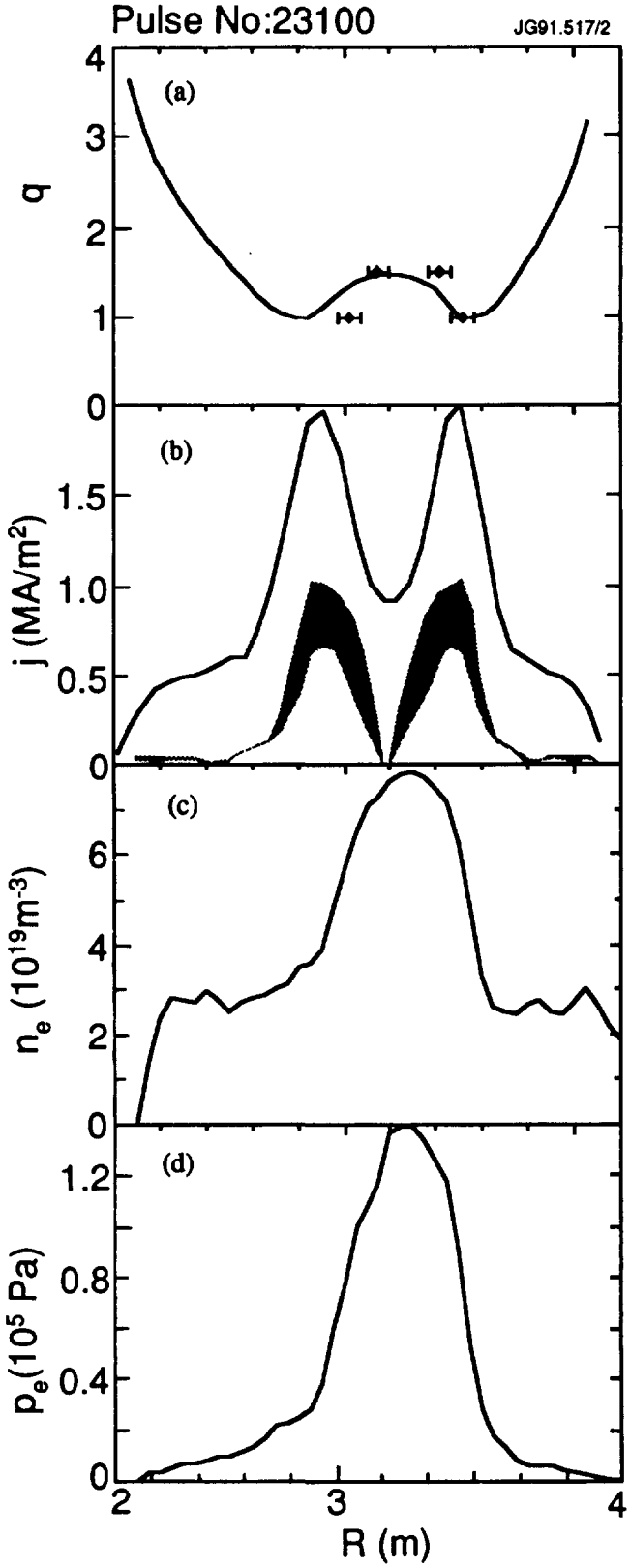

Fig.5 Computed and measured profiles for Pulse No.23100 at t = 6.605 s: (a) q-profile calculated using IDENTD and rational q-values determined from soft X-ray data analysis; (b) current density profile, averaged over the flux surfaces, obtained from IDENTD and bootstrap current contribution to the total current. The indicated shaded area reflects the uncertainty in the bootstrap current calculated from the local gradients of the measured LIDAR density and temperature profiles; (c) LIDAR electron density profile; (d) LIDAR electron pressure profile.

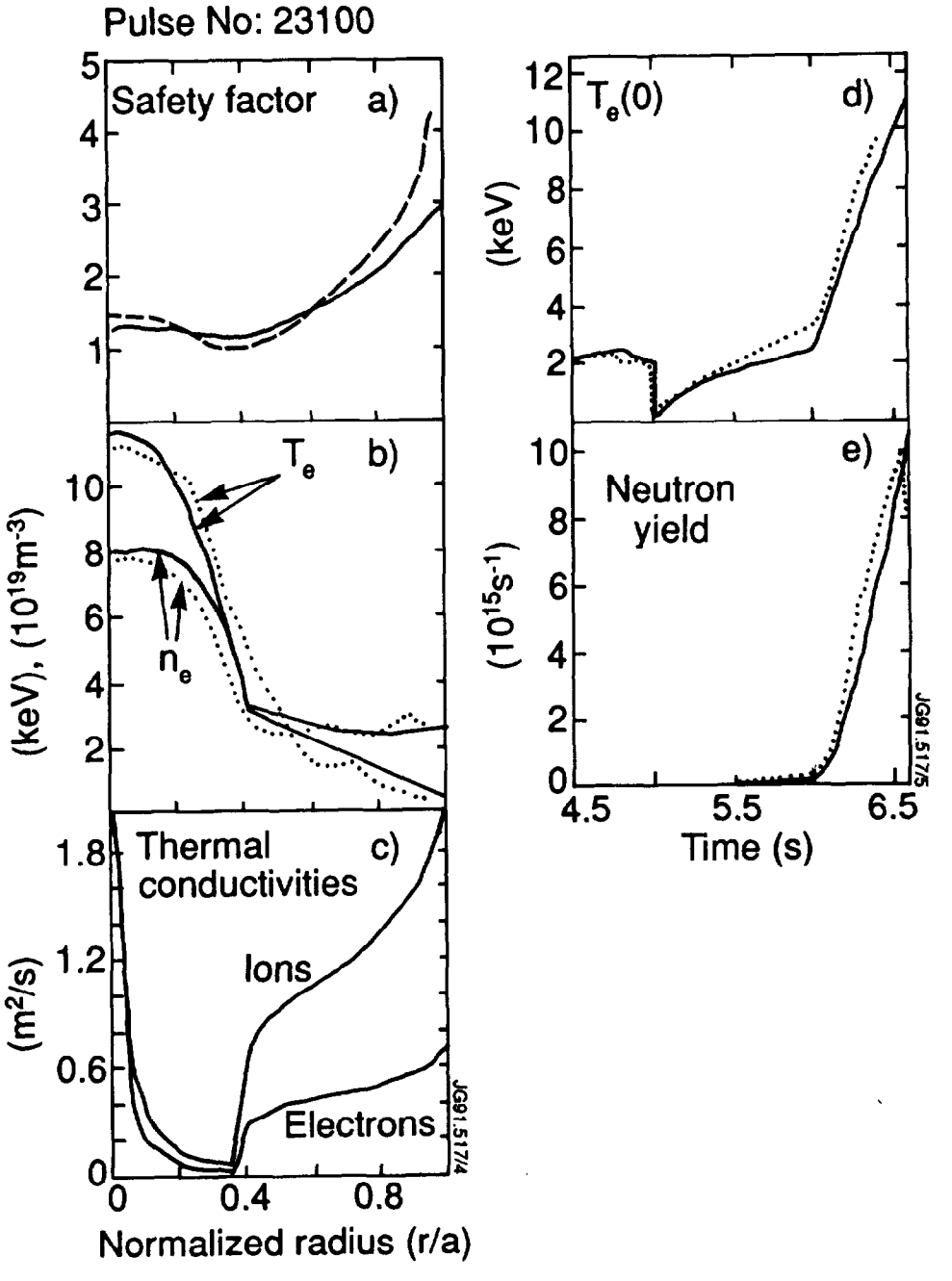

Fig.6 Results of a PEP pulse simulation obtained with a time dependent 1-D transport code (solid curves). (a) The dashed curve is the q-profile calculated by IDENTD. (b) The dotted curves are the LIDAR measurements of electron temperature T_e and density n_e profiles. (c) The transport is reduced within the region of negative shear as shown by the lower thermal conductivities. (d) The dotted line is the central electron temperature $T_e(0)$ measured by the Michelson interferometer as a function of time. (e) The dotted curve is the experimental neutron yield versus time.

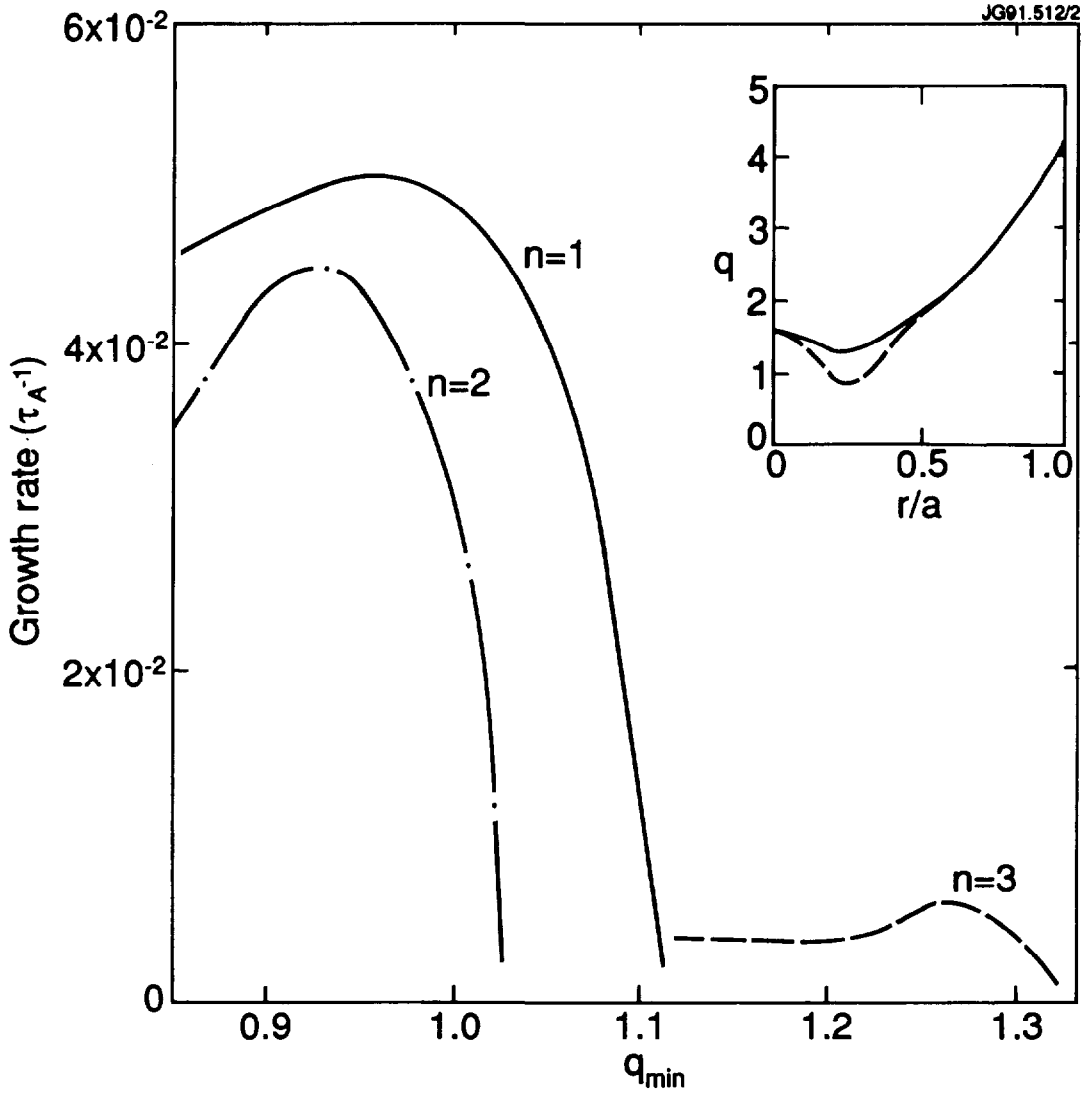

Fig.7 The growth rate of instabilities with toroidal mode numbers n = 1, 2 and 3, computed for a range of q-profiles. Non-monotonic q-profiles are used with a q on axis of 1.6 and an off-axis minimum q_{min} at r/a = 0.3. An example of some of these q-profiles is shown in the inset.

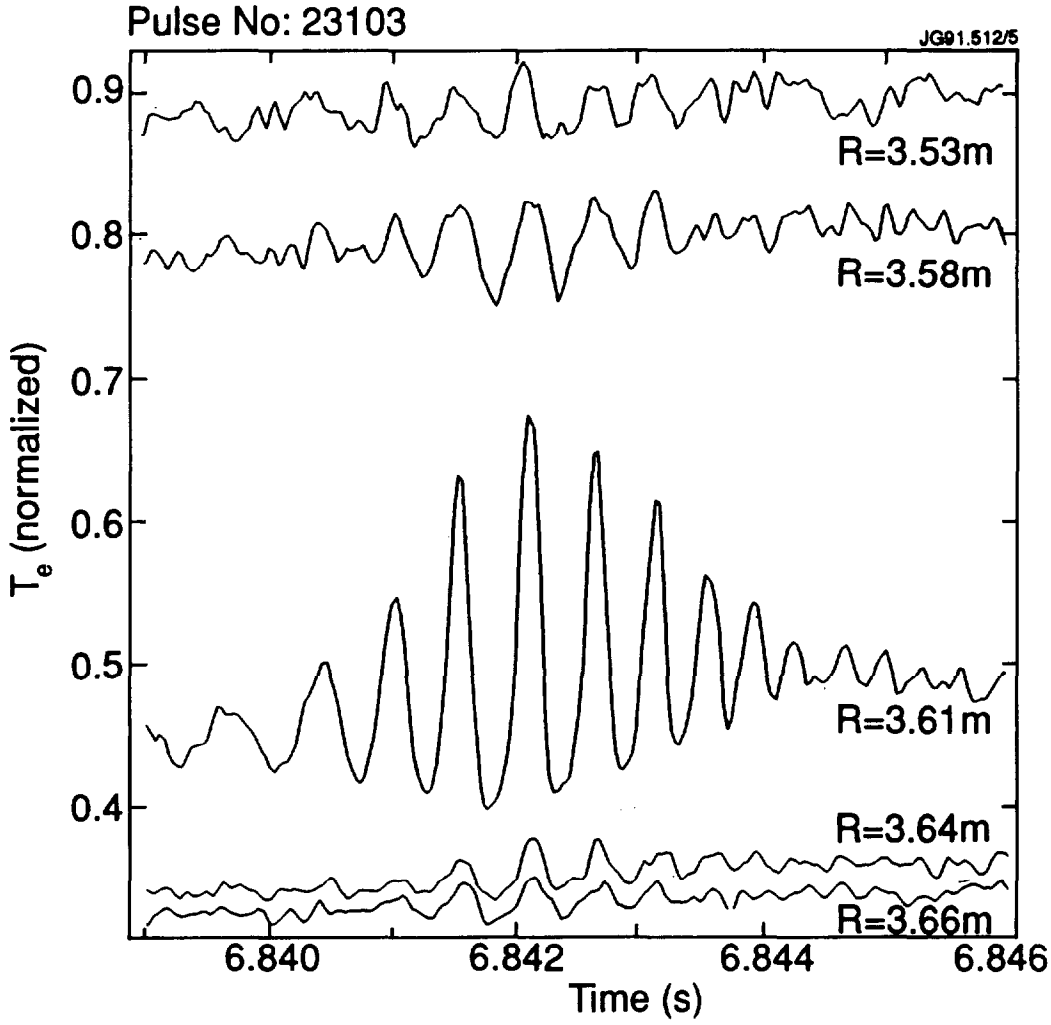

Fig.8 Electron temperature versus time as measured by various channels of the ECE radiometer. Note the large amplitude of the oscillations at R = 3.61 m and their non-sinusoidal behaviour. Due to difficulties in the absolute calibration for this pulse, only normalized temperatures are shown. The relative (channel-to-channel) uncertainty in the profile is $\pm$ 5 %.

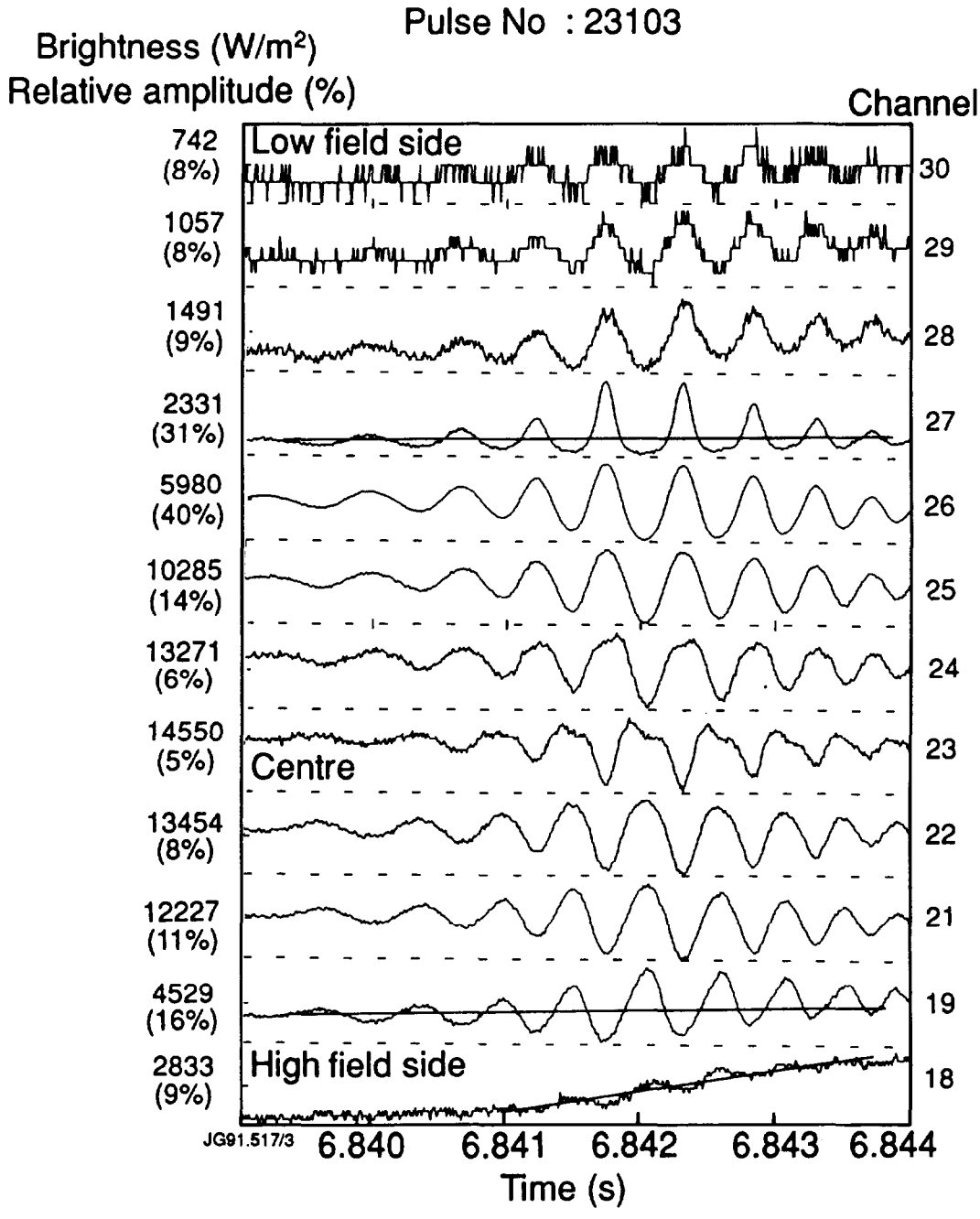

Fig.9 Line integrated soft X-ray emissivity measured by the vertical camera showing the ballooning character of the (1,1) mode. The brightness measured in W/m^2 by each channel is given with the relative amplitude of the oscillation. The plasma centre at R ≈ 3.30 m is viewed by channel 23. The (1,1) mode amplitude is larger on the low-field side (channel 27) than on the high-field side (intermediate between channels 18 and 19).

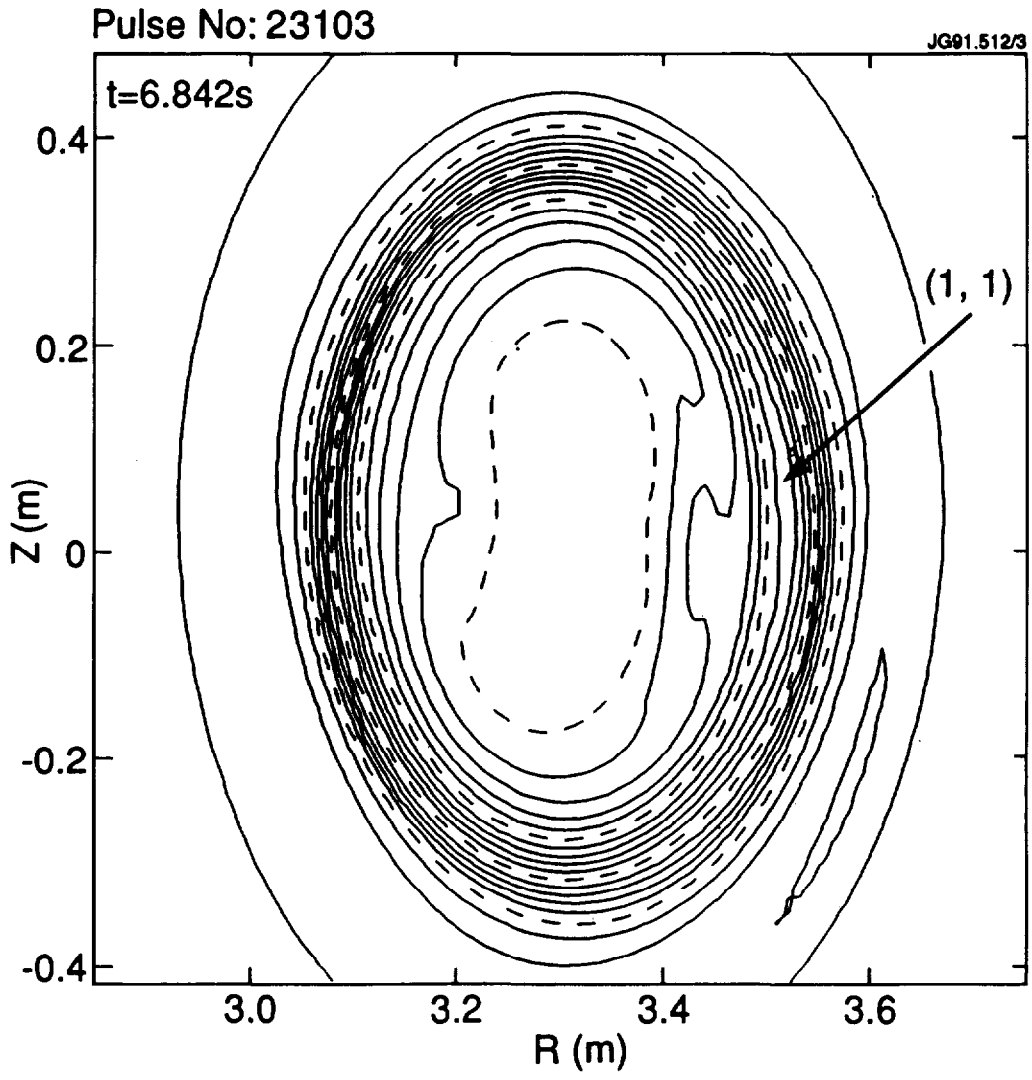

Fig.10 Rotational tomographic reconstruction of the soft X-ray emissivity showing an (m,n) = (1,1) mode.

APPENDIX 1.

THE JET TEAM

JET Joint Undertaking, Abingdon, Oxon, OX14 3EA, U.K.

J.M.Adams[1], F.Alladio[4], H.Altmann, R.J.Anderson, G.Appruzzese, W.Bailey, B.Balet, D.V.Bartlett, L.R.Baylor[24], K.Behringer, A.C.Bell, P.Bertoldi, E.Bertolini, V.Bhatnagar, R.J.Bickerton, A.Boileau[3], T.Bonicelli, S.J.Booth, G.Bosia, M.Botman, D.Boyd[31], H.Brelen, H.Brinkschulte, M.Brusati, T.Budd, M.Bures, T.Businaro[4], H.Buttgereit, D.Cacaut, C.Caldwell-Nichols, D.J.Campbell, P.Card, J.Carwardine, G.Celentano, P.Chabert[27], C.D.Challis, A.Cheetham, J.Christiansen, C.Christodoulopoulos, P.Chuilon, R.Claesen, S.Clement[30], J.P.Coad, P.Colestock[6], S.Conroy[13], M.Cooke, S.Cooper, J.G.Cordey, W.Core, S.Corti, A.E.Costley, G.Cottrell, M.Cox[7], P.Cripwell[13], F.Crisanti[4], D.Cross, H.de Blank[16], J.de Haas[16], L.de Kock, E.Deksnis, G.B.Denne, G.Deschamps, G.Devillars, K.J.Dietz, J.Dobbing, S.E.Dorling, P.G.Doyle, D.F.Düchs, H.Duquenoy, A.Edwards, J.Ehrenberg[14], T.Elevant[12], W.Engelhardt, S.K.Erents[7], L.G.Eriksonn[5], M.Evrard[2], H.Falter, D.Flory, M.Forrest[7], C.Froger, K.Fullard, M.Gadeberg[11], A.Galetsas, R.Galvao[8], A.Gibson, R.D.Gill, A.Gondhalekar, C.Gordon, G.Gorini, C.Gormezano, N.A.Gottardi, C.Gowers, B.J.Green, F.S.Griph, M.Gryzinski[26], R.Haange, G.Hammett[6], W.Han[9], C.J.Hancock, P.J.Harbour, N.C.Hawkes[7], P.Haynes[7], T.Hellsten, J.L.Hemmerich, R.Hemsworth, R.F.Herzog, K.Hirsch[14], J.Hoekzema, W.A.Houlberg[24], J.How, M.Huart, A.Hubbard, T.P.Hughes[32], M.Hugon, M.Huguet, J.Jacquinot, O.N.Jarvis, T.C.Jernigan[24], E.Joffrin, E.M.Jones, L.P.D.F.Jones, T.T.C.Jones, J.Källne, A.Kaye, B.E.Keen, M.Keilhacker, G.J.Kelly, A.Khare[15], S.Knowlton, A.Konstantellos, M.Kovanen[21], P.Kupschus, P.Lallia, J.R.Last, L.Lauro-Taroni, M.Laux[33], K.Lawson[7], E.Lazzaro, M.Lennholm, X.Litaudon, P.Lomas, M.Lorentz-Gottardi[2], C.Lowry, G.Magyar, D.Maisonnier, M.Malacarne, V.Marchese, P.Massmann, L.McCarthy[28], G.McCracken[7], P.Mendonca, P.Meriguet, P.Micozzi[4], S.F.Mills, P.Millward, S.L.Milora[24], A.Moissonnier, P.L.Mondino, D.Moreau[17], P.Morgan, H.Morsi[14], G.Murphy, M.F.Nave, M.Newman, L.Nickesson, P.Nielsen, P.Noll, W.Obert, D.O'Brien, J.O'Rourke, M.G.Pacco-Düchs, M.Pain, S.Papastergiou, D.Pasini[20], M.Paume[27], N.Peacock[7], D.Pearson[13], F.Pegoraro, M.Pick, S.Pitcher[7], J.Plancoulaine, J-P.Poffé, F.Porcelli, R.Prentice, T.Raimondi, J.Ramette[17], J.M.Rax[27], C.Raymond, P-H.Rebut, J.Removille, F.Rimini, D.Robinson[7], A.Rolfe, R.T.Ross, L.Rossi, G.Rupprecht[14], R.Rushton, P.Rutter, H.C.Sack, G.Sadler, N.Salmon[13], H.Salzmann[14], A.Santagiustina, D.Schissel[25], P.H.Schild, M.Schmid, G.Schmidt[6], R.L.Shaw, A.Sibley, R.Simonini, J.Sips[16], P.Smeulders, J.Snipes, S.Sommers, L.Sonnerup, K.Sonnenberg, M.Stamp, P.Stangeby[19], D.Start, C.A.Steed, D.Stork, P.E.Stott, T.E.Stringer, D.Stubberfield, T.Sugie[18], D.Summers, H.Summers[20], J.Taboda-Duarte[22], J.Tagle[30], H.Tamnen, A.Tanga, A.Taroni, C.Tebaldi[23], A.Tesini, P.R.Thomas, E.Thompson, K.Thomsen[11], P.Trevalion, M.Tschudin, B.Tubbing, K.Uchino[29], E.Usselmann, H.van der Beken, M.von Hellermann, T.Wade, C.Walker, B.A.Wallander, M.Walravens, K.Walter, D.Ward, M.L.Watkins, J.Wesson, D.H.Wheeler, J.Wilks, U.Willen[12], D.Wilson, T.Winkel, C.Woodward, M.Wykes, I.D.Young, L.Zannelli, M.Zarnstorff[6], D.Zasche[14], J.W.Zwart.

PERMANENT ADDRESS

1. UKAEA, Harwell, Oxon. UK.
2. EUR-EB Association, LPP-ERM/KMS, B-1040 Brussels, Belgium.
3. Institute National des Récherches Scientifique, Quebec, Canada.
4. ENEA-CENTRO Di Frascati, I-00044 Frascati, Roma, Italy.
5. Chalmers University of Technology, Göteborg, Sweden.
6. Princeton Plasma Physics Laboratory, New Jersey, USA.
7. UKAEA Culham Laboratory, Abingdon, Oxon. UK.
8. Plasma Physics Laboratory, Space Research Institute, Sao José dos Campos, Brazil.
9. Institute of Mathematics, University of Oxford, UK.
10. CRPP/EPFL, 21 Avenue des Bains, CH-1007 Lausanne, Switzerland.
11. Risø National Laboratory, DK-4000 Roskilde, Denmark.
12. Swedish Energy Research Commission, S-10072 Stockholm, Sweden.
13. Imperial College of Science and Technology, University of London, UK.
14. Max Planck Institut für Plasmaphysik, D-8046 Garching bei München, FRG.
15. Institute for Plasma Research, Gandhinagar Bhat Gujat, India.
16. FOM Instituut voor Plasmafysica, 3430 Be Nieuwegein, The Netherlands.
17. Commissiariat à L'Energie Atomique, F-92260 Fontenay-aux-Roses, France.
18. JAERI, Tokai Research Establishment, Tokai-Mura, Naka-Gun, Japan.
19. Institute for Aerospace Studies, University of Toronto, Downsview, Ontario, Canada.
20. University of Strathclyde, Glasgow, G4 ONG, U.K.
21. Nuclear Engineering Laboratory, Lapeenranta University, Finland.
22. JNICT, Lisboa, Portugal.
23. Department of Mathematics, Univeristy of Bologna, Italy.
24. Oak Ridge National Laboratory, Oak Ridge, Tenn., USA.
25. G.A. Technologies, San Diego, California, USA.
26. Institute for Nuclear Studies, Swierk, Poland.
27. Commissiariat à l'Energie Atomique, Cadarache, France.
28. School of Physical Sciences, Flinders University of South Australia, South Australia SO42.
29. Kyushi University, Kasagu Fukuoka, Japan.
30. Centro de Investigaciones Energeticas Medioambientales y Techalogicas, Spain.
31. University of Maryland, College Park, Maryland, USA.
32. University of Essex, Colchester, UK.
33. Akademie de Wissenschaften, Berlin, DDR.

CR 88.49.1A